Optics & Laser Technology 41 (2009) 241–246

Contents lists available at ScienceDirect

Optics & Laser Technology

journal homepage: www.elsevier.com/locate/optlastec

Focus shaping of cylindrically polarized vortex beams by a high numerical-aperture lens

Lianzhou Rao [a,*], Jixiong Pu [b], Zhiyang Chen [b], Pu Yei [a]

[a] Department of Physics and Electromechanical Engineering, Sanming University, Sanming, Fujian 365004, China
[b] Department of Electronic Science and Technology, Huaqiao University, Quanzhou, Fujian 362021, China

ARTICLE INFO

Article history:
Received 25 August 2007
Received in revised form
18 June 2008
Accepted 30 June 2008
Available online 8 August 2008

PACS:
42.25.−p
42.25.Ja

Keywords:
Wave optics
Beam shaping
Polarization

ABSTRACT

The focus-shaping technique of a cylindrically polarized vortex beam by a high numerical-aperture lens is reported. Such a polarized vortex beam is decomposed into radial and azimuthal polarization. It is shown that the total intensity distribution in the focal region is dependent not only on the numerical-aperture maximal angle and the polarization rotation angle but also on the topological charge. By choosing the proper combination of parameters, the adjustably confined flat-topped focus and focal hole can be obtained. The focus-shaping technique may find wide applications, such as optical tweezers, laser printing and material processing.

© 2008 Elsevier Ltd. All rights reserved.

1. Introduction

Study and applications of the optical vortex beam have recently generated great research interest, which has resulted in a new branch of singular optics in modern optics [1–7]. Optical vortex beams possess wave-front dislocations, where the phase values are undefined (also referred to as phase singularities) and the amplitude vanishes to zero. Such beams can be generated by using the spatial light modulators (SLMs) or the spatial phases plates (SPPs) [3] and possess a helical phase structure of $\exp(\mathrm{i}n\phi)$, where ϕ is the polar coordinate in the plane perpendicular to the beam axis and n is the so-called topological charge. It is further known that such an optical vortex beam carries orbital angular momentum (OAM) and each photon has a magnitude of $n\hbar$ OAM [4,5] and can be used to trap and rotate particles [6]. On the other hand, the radially and the azimuthally polarized beams are of particular importance in many application fields due to the unique cylindrical symmetry of polarization. Various methods for generation of such polarized beams have been suggested. For instance, the alternative methods include twisted nematic liquid crystals with specially designed alignment layers [8], segmented filters with properly oriented half-wave plates [9] and so on. Recently, the focusing properties of a polarized beam and a circularly, radially, azimuthally or linearly polarized vortex beam by a high numerical-aperture (NA) lens have been discussed [10–16]. The study of coherent superposition of radially and azimuthally polarized components has also generated interest [21]. As yet, to the best of our knowledge, the focus shaping of a cylindrically polarized vortex beam by a high NA lens is little studied. With an increasing number of new applications, it is of great importance to explore the focus shaping of such polarized vortex beams.

In this paper, we study the focus-shaping technique of a cylindrically polarized vortex beam by a high NA lens. Such a beam can be generated by the combination of SLM and two half-wave plates and can be decomposed into a linear superposition of radially polarized and azimuthally polarized components. Numerical simulation shows that total intensity distribution in the vicinity of the focus is dependent not only on the NA maximal angle and the polarization rotation angle but also on the topological charge n. The adjustably confined flat-topped focus and focal hole can be obtained by choosing the proper combination of parameters. Specifically, an added advantage of using an optical vortex beam is that it allows us to transfer angular momentum to atoms and colloids, thus opening up new applications of such small flat-topped focus and focal holes.

* Corresponding author. Fax: +86 598 8397250.
E-mail address: 8310176@163.com (L. Rao).

0030-3992/$ - see front matter © 2008 Elsevier Ltd. All rights reserved.
doi:10.1016/j.optlastec.2008.06.012

2. Theoretical model

The optical vortex beam possessing cylindrical polarization is generated by a beam passing SLM and polarization rotator. Fig. 1 shows the polarization pattern of the polarization rotator. Instead of a radial polarization or an azimuthal polarization, each point of the optical vortex beam has a polarization rotated by ϕ_0 from its radial direction. A simple polarization rotator consisting of two half-wave plates can be used to perform such a conversion [14,18]. By simply rotating one of the half-wave plates, we can control the polarization rotation angle ϕ_0 of the optical vortex beam. Thus, the optical vortex beam possessing cylindrical polarization can be expressed as $\boldsymbol{E}_{\text{in}} = AP(r)\exp(in\varphi)(\cos\phi_0\boldsymbol{e}_r+\sin\phi_0\boldsymbol{e}_\varphi)$, where $P(r)$ is the axially symmetric amplitude distribution of the beam and A is a constant. Since the optical vortex beam possesses cylindrical polarization, such beam may appropriately be called a cylindrically polarized vortex beam. In contrast to a cylindrical vector beam, the phase of the cylindrically polarized vortex beam is helical: there is a phase difference between different points of the beam profile and the cylindrically polarized vortex beam has OAM. If the beam is the no-vortex mode (i.e., $n = 0$), then the resulting beam will be a degenerate cylindrical vector beam mode, which has no OAM.

In this paper, we assume that the cylindrically polarized vortex beam is incident upon a high NA lens. Since this beam can be expressed as a linear superposition of radial polarization and azimuthal polarization, the field near the focus can be expressed as a linear combination of the focal fields of radial polarization and azimuthal polarization. Using the same analysis method as that in Refs. [14,19,20], the focal field of a cylindrically polarized vortex beam can be written as

$$\boldsymbol{E}_{\text{out}}(r,\varphi,z) = E_r\boldsymbol{e}_r + E_z\boldsymbol{e}_z + E_\varphi\boldsymbol{e}_\varphi, \tag{1}$$

where $\boldsymbol{e}_r$, $\boldsymbol{e}_z$ and $\boldsymbol{e}_\varphi$ are the unit vector in the radial, longitudinal and azimuthal directions, respectively. E_r, E_z, and E_φ are the amplitudes of the three orthogonal components, respectively and can be expressed as

$$E_r(r,\varphi,z) = \frac{-\mathrm{i}A}{2\pi}\cos\phi_0\int_0^\alpha\int_0^{2\pi}\sqrt{\cos\theta}\sin(2\theta)P(\theta) \times\cos(\phi-\varphi)\exp(\mathrm{i}n\phi)\exp[\mathrm{i}k(z\cos\theta + r\sin\theta\cos(\phi-\varphi))]\,\mathrm{d}\phi\,\mathrm{d}\varphi \tag{2}$$

$$E_z(r,\varphi,z) = \frac{\mathrm{i}A}{\pi}\cos\phi_0\int_0^\alpha\int_0^{2\pi}\sqrt{\cos\theta}\sin^2\theta P(\theta)\exp(\mathrm{i}n\phi) \times\exp[\mathrm{i}k(z\cos\theta + r\sin\theta\cos(\phi-\varphi))]\,\mathrm{d}\phi\,\mathrm{d}\theta, \tag{3}$$

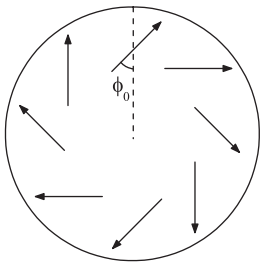

Fig. 1. The polarization pattern of the polarization rotator. An optical vortex beam passes the polarization rotator, as a result the vortex beam possess cylindrical polarization. ϕ_0 is the polarization rotation angle from the purely radial polarization.

$$E_\phi(r,\varphi,z) = \frac{-\mathrm{i}A}{\pi}\sin\phi_0\int_0^\alpha\int_0^{2\pi}\sqrt{\cos\theta}\sin\theta P(\theta) \times\cos(\phi-\varphi)\exp(\mathrm{i}n\phi)\exp[\mathrm{i}k(z\cos\theta + r\sin\theta\cos(\phi-\varphi))]\,\mathrm{d}\phi\,\mathrm{d}\theta \tag{4}$$

Using the following formulae:

$$\int_0^{2\pi}\exp[\mathrm{i}n\phi + \mathrm{i}kr\sin\theta\cos(\phi-\varphi)]\,\mathrm{d}\phi = 2\pi i^n\exp(\mathrm{i}n\varphi)J_n(kr\sin\theta), \tag{5}$$

$$\int_0^{2\pi}\cos(\phi-\varphi)\exp[\mathrm{i}n\phi + \mathrm{i}kr\sin\theta\cos(\phi-\varphi)]\,\mathrm{d}\phi = \pi i^{n+1}\exp(\mathrm{i}n\varphi)[J_{n+1}(kr\sin\theta) - J_{n-1}(kr\sin\theta)], \tag{6}$$

We obtain the following expressions:

$$E_r(r,\varphi,z) = \frac{i^nA}{2}\exp(\mathrm{i}n\varphi)\cos\phi_0\int_0^\alpha\sqrt{\cos\theta}\sin(2\theta)P(\theta) \times\exp[\mathrm{i}k(z\cos\theta)][J_{n+1}(kr\sin\theta) - J_{n-1}(kr\sin\theta)]\,\mathrm{d}\theta, \tag{7}$$

$$E_z(r,\varphi,z) = 2i^{n+1}A\exp(\mathrm{i}n\varphi)\cos\phi_0\int_0^\alpha\sqrt{\cos\theta}\sin^2\theta P(\theta) \times\exp[\mathrm{i}k(z\cos\theta)]J_n(kr\sin\theta)\,\mathrm{d}\theta, \tag{8}$$

$$E_\varphi(r,\varphi,z) = i^nA\exp(\mathrm{i}n\varphi)\sin\phi_0\int_0^\alpha\sqrt{\cos\theta}\sin\theta P(\theta) \times\exp[\mathrm{i}k(z\cos\theta)][J_{n+1}(kr\sin\theta) - J_{n-1}(kr\sin\theta)]\,\mathrm{d}\theta \tag{9}$$

where r, φ and z are the radial, azimuthal and longitudinal coordinates of the observation point in the focal region, respectively. $k = 2\pi/\lambda$ is wave number, $P(\theta)$ is the pupil apodization function and $\alpha = \sin^{-1}(\text{NA})$ is the maximal angle determined by the numerical aperture of the lens. J_n, J_{n+1} and J_{n-1} the Bessel function of the first kind with order n, n+1 and n−1, respectively. n is the topological charge of the vortex beam. Note that all optical intensity are independent of φ, which means the intensity distribution maintains cylindrical symmetry. With these Eqs. (7)–(9), we can calculate the intensity distribution corresponding to different components (E_r, E_z and E_φ) as well as the total intensity in the vicinity of focus. For all the examples in this paper, we choose as $P(\theta) = 1$, $A = 1$. The polarization rotation angle ϕ_0 changes from 0 to $\pi/2$ and the length unit is normalized to wavelength λ.

3. Focus shaping and numerical simulation

3.1. Radially and azimuthally polarized vortex beams

Fig. 2(a) shows the intensity distribution in the focal plane for $\phi_0 = 0^\circ$, $\text{NA} = \sin(80^\circ)$ and topological charge $n = 1$, which corresponds to a radially polarized vortex incident beam. The two-dimensional intensity distributions at the vicinity of the focus are shown in Fig. 2(b–d). In Fig. 2, the more whiteness indicates the higher intensity (the same applies to the other figures). The total intensity is the sum of the azimuthal intensity, radial intensity and longitudinal intensity. In this case, the azimuthal component disappears and only the radial and longitudinal components are present. One can see that the radial component distribution is a highly confined focal spot and the longitudinal component distribution is a highly confined focal hole. The radial component has only half of the width (approximately) of the total intensity distribution, and the total intensity is nonzero on the optical axis [11,15]. In contrast to the

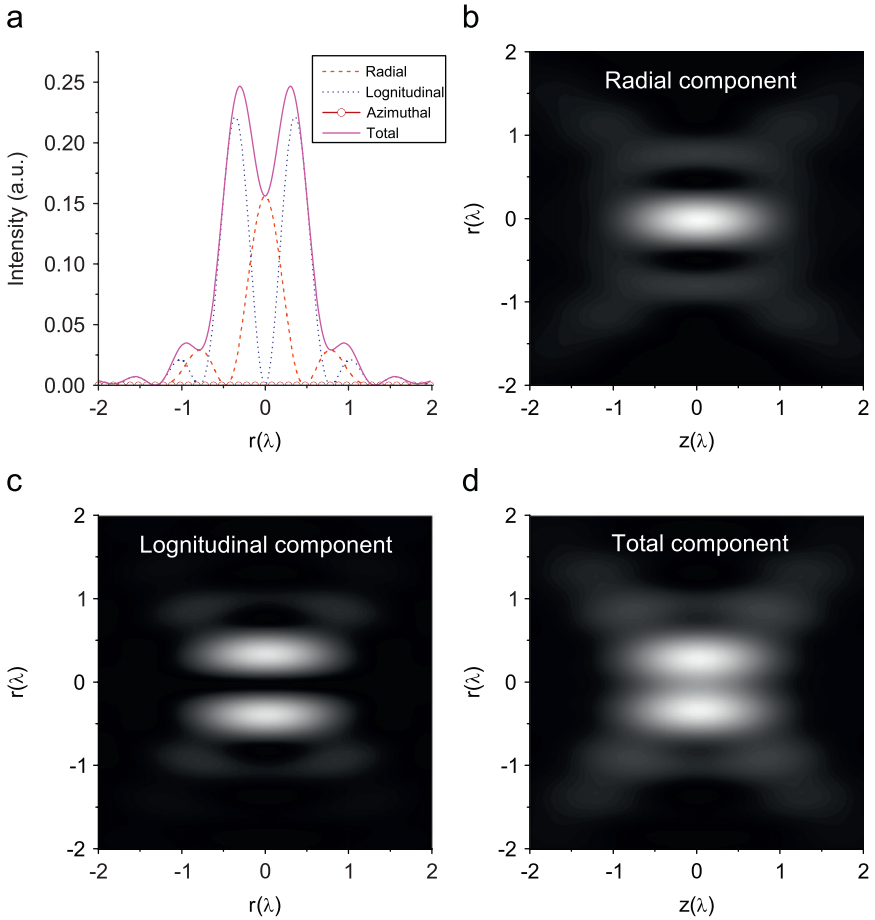

Fig. 2. (a) Intensity distribution at the focal plane and (b)–(d) intensity distribution in the vicinity of the focus for a radially polarized vortex beam. The parameters are chosen as $n = 1$, $\alpha = \sin^{-1}(\mathrm{NA}) = 80^\circ$, $\phi_0 = 90^\circ$.

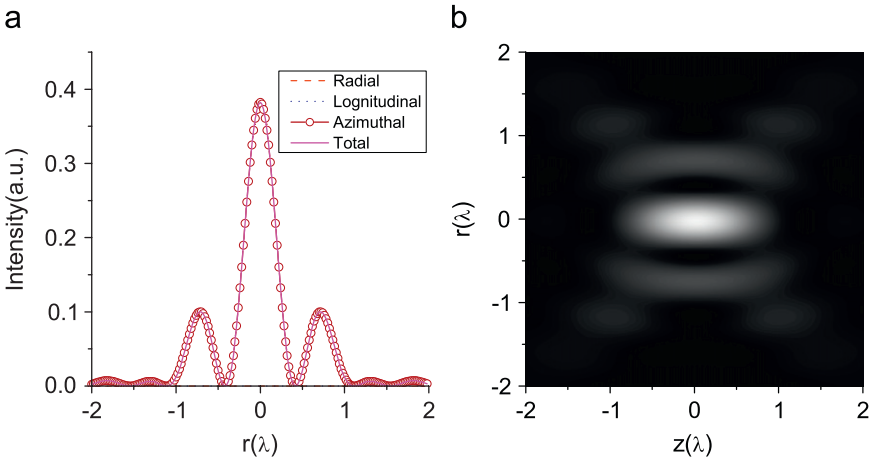

Fig. 3. (a) Intensity distribution at the focal plane and (b) total intensity distribution in the vicinity of focus for an azimuthally polarized vortex beam. The focal field only has an azimuthal component. The radial and longitudinal components are zero. Here $\phi_0 = 90^\circ$ and the other parameters are the same as those in Fig. 2.

focus profiles for the radial case (i.e., $n = 0$ case) discussed in Refs. [9,14,20], the focus profiles for the radially polarized vortex beam (i.e., $n = 1$ case) are different. That is, the longitudinal component distribution has an on-axis minimum (see Fig. 2c). This phenomenon is easily understood by analyzing the Bessel function J_n of Eq. (8).

Fig. 3(a) plots the intensity distribution in the focal plane for $\phi_0 = 90^\circ$, $NA = \sin(80^\circ)$ and $n = 1$, which correspond to an azimuthally polarized vortex incident beam. The two-dimensional intensity distribution is shown in Fig. 3(b). It is seen that the azimuthally polarized vortex beam has no radial and longitudinal component and the total intensity distribution on the optical axis has a maximum [11]. Hence, such azimuthally polarized vortex beams can obtain a highly confined focal spot. The focal spot size (0.39λ, $\alpha = 90^\circ$) is slightly larger than that obtained in Ref. [12] (smallest focal spot: 0.36λ, $\alpha = 90^\circ$). However, in our study, the

incident beam is a vortex one, so that the focal spot possesses OAM. However, it must be emphasized that this result for $n = 1$ is contrary to that for $n = 0$ analyzed in Refs. [14,20]. This behavior is easily understood by analyzing the Bessel functions J_{n+1} and J_{n-1} of Eq. (9). When $r = 0$, substituting Eq. (9) into Eq. (1) gives

$$\begin{aligned}\boldsymbol{E}_{\text{out}}(r,\varphi,z) &= E_\varphi(r,\varphi,z)\boldsymbol{e}_\varphi = [\mathrm{i}A\exp(\mathrm{i}\varphi)\int_0^\alpha \sqrt{\cos\theta}\sin\theta P(\theta)\\ &\quad\times\exp[\mathrm{i}k(z\cos\theta)]\,\mathrm{d}\theta]\boldsymbol{e}_\varphi\\ &= A(\mathrm{i}\cos\varphi\boldsymbol{e}_\varphi - \sin\varphi\boldsymbol{e}_\varphi)\\ &\quad\times\int_0^\alpha \sqrt{\cos\theta}\sin\theta P(\theta)\exp[\mathrm{i}k(z\cos\theta)]\,\mathrm{d}\theta \end{aligned} \tag{10}$$

Thus, in this part of the focal region, the wavefield is circularly polarized and the axial intensity is here equivalent to that of an ordinary beam without vortices. From Eq. (9), we can also note that $n = 1$ is the only value of n that gives rise to a nonzero optical intensity on the optical axis.

3.2. Flat-topped focus

From Figs. 2 and 3, we notice that the longitudinal polarization component has only one focal hole in the focal region. For the radial and azimuthal polarization components, however, focal spots are located in the center of the focal hole. Because the size of this focal spot is similar to the size of the dark core of the focal hole, we can obtain a flat-topped total intensity distribution at the focus by adjusting the weightings of the three-field components by adjusting ϕ_0. This adjusting of ϕ_0 can be achieved using the pure polarization rotators, as described previously. Fig. 4(a and c) shows the intensity distribution in the focal plane for $\phi_0 = 0°$, NA $= \sin(60°)$ and $\phi_0 = 31.2°$, NA $= \sin(80°)$, which correspond to a cylindrically polarized vortex incident beam. The two-dimensional total intensity through the focus (in the r–z plane) is shown in Fig. 4(b and d). One can see that the flat-topped total intensity distribution in the focal plane is obtained by adjusting the two parameters ϕ_0 and α. The flat-topped focus sizes for different

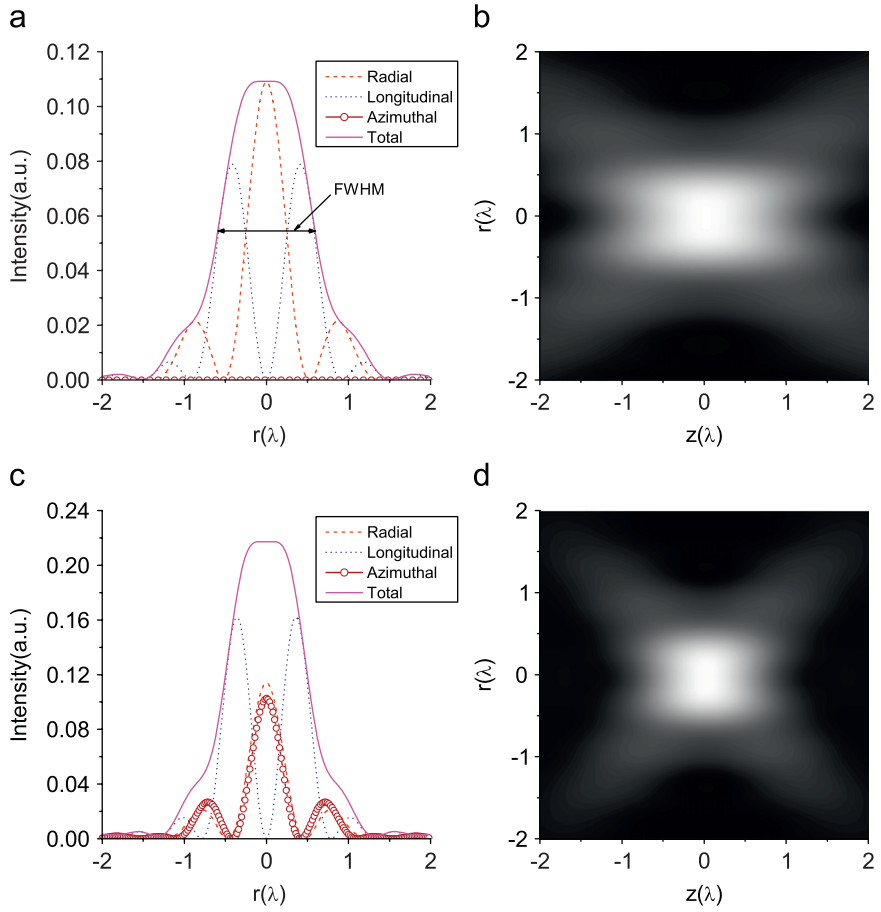

Fig. 4. (a), (c) Intensity distribution at the focal plane, (b) and (d) total intensity distribution in the vicinity of focus for different values of α and ϕ_0. Here (a), (b) $\phi_0 = 90°$, $\alpha = \sin^{-1}(\mathrm{NA}) = 60°$; (c), (d) $\phi_0 = 31.2°$, $\alpha = \sin^{-1}(\mathrm{NA}) = 80°$. The other parameters are the same as those in Fig. 2.

Table 1
Comparison of the flat-topped focus sizes for different values of α and n

NA maximal angle α (deg)		60	65	70	75	80	90
Polarization rotation angle ϕ_0 (deg)	$n = 1$	0	17	24	28.2	31.2	34.2
Flat-topped focus size (λ)		1.18	1.14	1.1	1.06	1.04	1.02
Polarization rotation angle ϕ_0 (deg)	$n = 0$	33	38	40.5	42.2	44.2	46.2
Flat-topped focus size (λ)		1.28	1.24	1.18	1.12	1.1	1.06

The flat-topped focus sizes denote full-width at half-maximum (FWHM) of total intensity profiles.

values of α and n are also shown in Table 1. Here the focus sizes denote full-width at half-maximum (FWHM) of total intensity profiles shown in Fig. 4(a). It is found that the flat-topped focus sizes decrease and the maximum intensity increases with the increase in α and ϕ_0. In contrast to cylindrical vector beams (i.e., $n=0$, no-vortex) [14], for a fixed α, the flat-topped focus size in the $n=1$ case (such as $\alpha=80^\circ$, FWHM $=1.04\lambda$) is smaller than the one obtained in the $n=0$ case (such as $\alpha=80^\circ$, FWHM $=1.1\lambda$) and each photon of the flat-topped focus in the $n=1$ case has an OAM of magnitude $\hbar$.

The flat-topped focus obtained above may find some applications such as improved printing filling factor, improved uniformity and quality in materials processing, micro-lithography, and so on. In our calculations, we have used a very simple pupil apodization function. However, the pupil apodization provides another degree of freedom to shape the focus. It is possible to improve the quality of the flat-topped focus by using a more complex pupil apodization function.

3.3. Focal hole

As shown above, we can note that $n=1$ or $n=0$ gives rise to a nonzero optical intensity on the optical axis. However, for all other topological charges $n>1$, the polarized vortex beam is zero on the optical axis due to destructive interference. Such behaviors are presented in Fig. 5 for different values of ϕ_0. In this case,

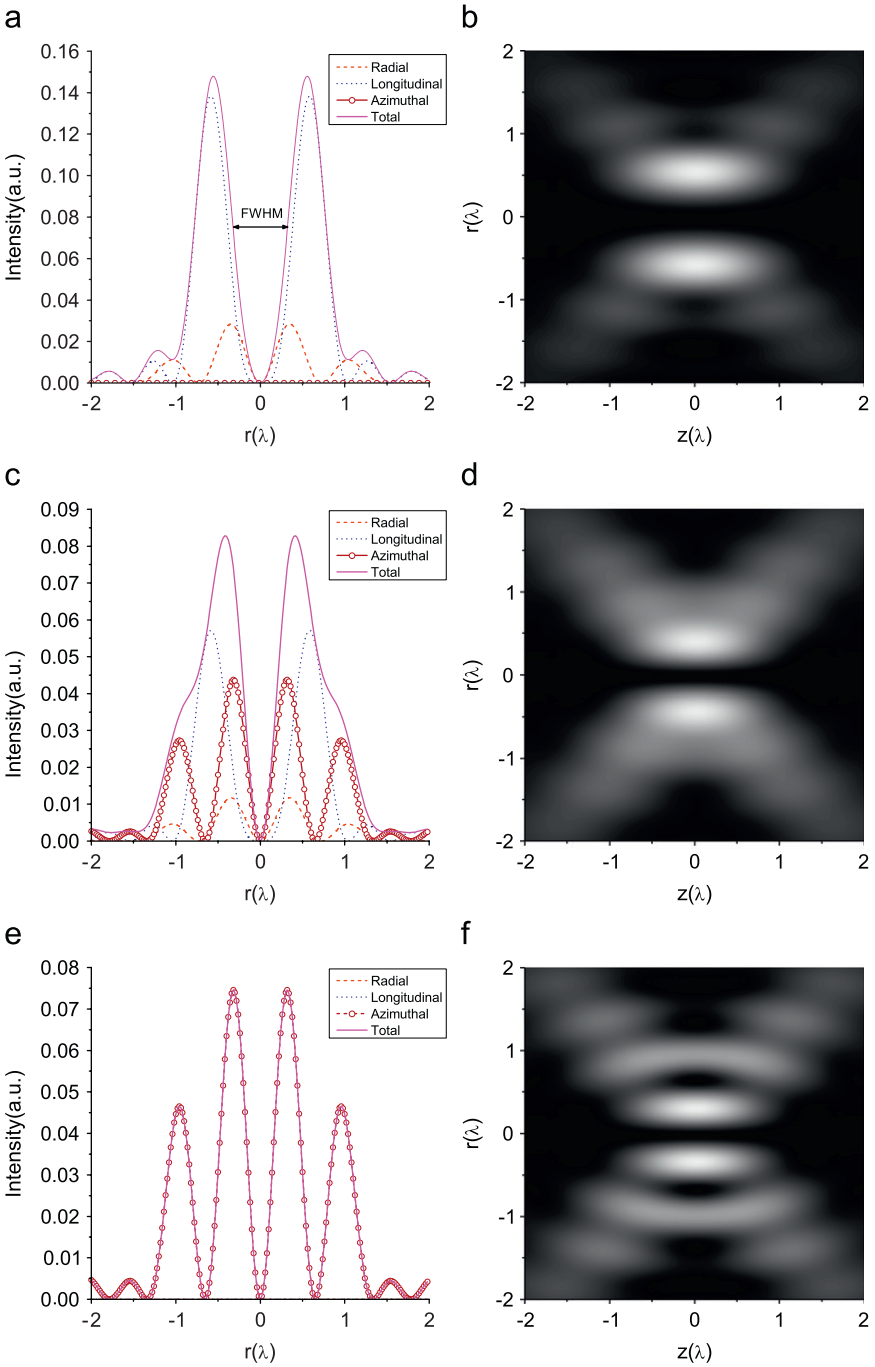

Fig. 5. (a), (c) and (e) Intensity distribution at the focal plane, (b), (d) and (f) total intensity distribution in the vicinity of focus for different values of ϕ_0. Here (a), (b) $\phi_0=0^\circ$; (c), (d) $\phi_0=50^\circ$; (e), (f) $\phi_0=90^\circ$. The other parameters are the same as those in Fig. 2.

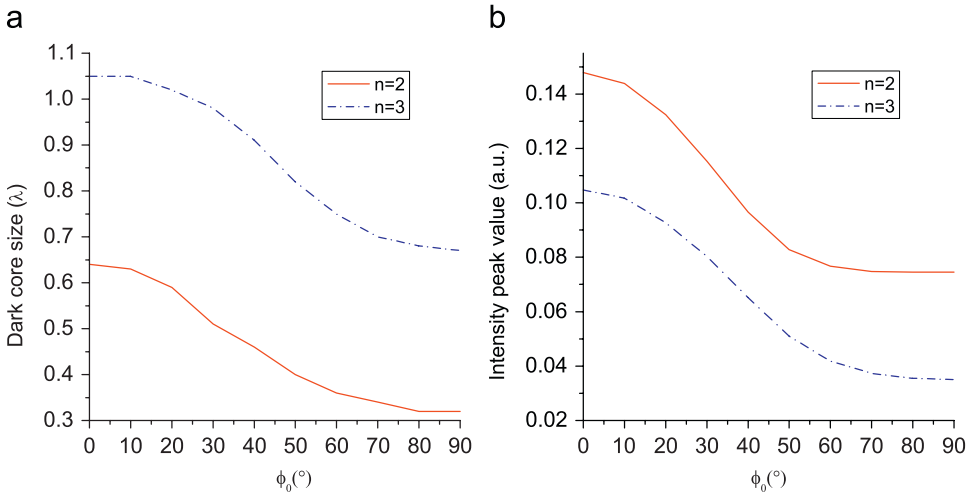

Fig. 6. (a) The focal hole size (FWHM) and (b), the intensity peak value at the focal plane for different values of n. Here $\alpha = \sin^{-1}(\mathrm{NA}) = 80^\circ$.

a dark channel along the optical axis, i.e., a focal hole, is achieved. It can be seen that the focal hole sizes (FWHM) reduce with the increase in ϕ_0. When ϕ_0 is from 0 to 50°, the side lobes are less pronounced; however, the side lobes become more pronounced as ϕ_0 continues to increase. Especially, when $\phi_0 = 90^\circ$(i.e., azimuthally polarized vortex), the FWHM is only 0.31λ ($\alpha = 90^\circ$), and the FWHM is almost the same as the one obtained using an azimuthally polarized beam combined with an annular phase filter (i.e., the smallest focal hole FWHM $= 0.3\lambda$, see Ref. [15]), although the first few side lobes are rather large. Thus, there is a tradeoff between side lobes and confinement and adjusting ϕ_0 may optimize this ratio. For example, when $\phi_0 = 50^\circ$ (Fig. 5c), the side lobes almost vanish and the FWHM $= 0.4\lambda$. Moreover, the focused light also belongs to the class of 'diffraction free' beams discussed in [17], and there is almost no broadening of the focal hole in the vicinity of the focal plane, and possesses the characteristics of the vortex. In addition, the focal hole sizes (FWHM) and the intensity peak values of the focal hole at the focal plane are shown in Fig. 6 for different values of n. It can be found that for a fixed ϕ_0 value, the focal hole sizes increase and the intensity peak values decrease with increasing n; and for a fixed n value, the larger the values of ϕ_0, the smaller the focal hole sizes and the intensity peak values.

Using the above-mentioned method, we can easily change the focal total intensity distribution from a focal spot shape to a controllable focal hole shape by adjusting the polarization rotation angle ϕ_0 and the topological charge n. Because such a focal hole possesses the characteristics of the vortex and also allows the transfer of angular momentum to a particle trapped or guided by the dark region, it may be used in a variety of particles guiding, trapping and inducing rotation.

4. Conclusions

We have described a novel beam-shaping technique—focus shaping—using cylindrically polarized vortex beams. It is shown that the total intensity distribution in the vicinity of the focus is dependent not only on the NA maximal angle α and the polarization rotation angle ϕ_0 but also on the topological charge n of the incident polarized vortex beams. At some particular conditions, the adjustably confined flat-topped focus can be generated for the $n = 1$ case. However, for all other topological charges $n > 1$, the adjustably confined focal hole can be obtained due to destructive interference. The focus-shaping technique may find wide applications, such as optical tweezers, laser printing and material processing.

Acknowledgements

This work was supported by the National Natural Science Foundation of China (Grant no. 60477041), the Natural Science Project of the Education Bureau of Fujian Province (Grant no. JA06048) and the Natural Science Project of Sanming University (Grant no. B0603/G), China.

References

[1] Nye JF, Berry MV. Proc R Soc London Ser A 1974;336:165.
[2] Soskin MS, Vasnetsov MV. A comprehensive review of optical vortices, in progress in optics, vol. 42. Amsterdam: Elsevier; 2001. 219.
[3] Kotlyar VV, Almazov AA, Khonina SN, Soifer VA. J Opt Soc Am A 2005;22:849.
[4] Palacios DM, Maleev ID, Marathay AS, Swartzlander Jr. GA. Phys Rev Lett 2004;92:143905.
[5] Tao SH, Yuan X-C, Lin J, Burge RE. Opt Express 2006;14:535.
[6] Kuga T, Torii Y, Shiokawa N, Hirano T, Shimizu Y, Sasada H. Phys Rev Lett 1997;78:4713.
[7] Rao L, Pu J. Chin Phys Lett 2007;24:1252.
[8] Stalder M, Schadt M. Opt Lett 1996;21:1948.
[9] Dorn R, Quabis S, Leuchs G. Phys Rev Lett 2003;91:233901.
[10] Quabis S, Dorn R, Eberler M, Glöckl O, Leuchs G. Appl Phys B 2001;72:109.
[11] Helseth LE. Opt Commun 2004;229:85.
[12] Grosjean T, Courjon D. Opt Commun 2007;272:314.
[13] Ganic D, Gan X, Gu M. Opt Express 2003;11:2747.
[14] Zhan Q, Leger JR. Opt Express 2002;10:324.
[15] Helseth LE. Opt Commun 2006;257:1.
[16] Zhan Q. Opt Lett 2006;31:867.
[17] Durnin J, Micelli JJ, Eberly JH. Phys Rev Lett 1987;58:1499.
[18] Niziev VG, Nesterov AV. J Phys D 1999;32:1455.
[19] Richards B, Wolf E. Proc R Soc London Ser A 1959;253:58.
[20] Youngworth KS, Brown TG. Opt Express 2000;7:77.
[21] Bokor N, Davidson N. Opt Commun 2007;279:229.